Lab on a Chip

Accepted Manuscript

ROYAL SOCIETY OF CHEMISTRY

www.rsc.org/loc

Simultaneous three-dimensional temperature and velocity field measurements using astigmatic imaging of non-encapsulated thermo-liquid crystal (TLC) particles†

Rodrigo Segura, Massimiliano Rossi, Christian Cierpka, and Christian J. Kähler

Received Xth XXXXXXXXXX 20XX, Accepted Xth XXXXXXXXX 20XX
First published on the web Xth XXXXXXXXXX 200X
DOI: 10.1039/b000000x

A combination of cutting edge developments is presented to characterize three-dimensional (3D) temperature and velocity fields in microscopic flows. An emulsion of non-encapsulated thermo-liquid crystal (TLC) micro spheres, with a narrow size distribution is used to track the flow's motion and temperature distribution. A state-of-the-art light engine, which combines the spectrum of six light pipes, provides a balanced illumination which allows for strong and detectable color patterns across the TLC's temperature response range. Lastly, the ability of the TLC material to reflect select wavelength bands with an unchanging and independent circular polarization chirality is exploited by a filter that blocks background noise, while exclusively transmitting the color signal of the TLC particles. This approach takes advantage of the peculiar physical properties of TLCs to allow the estimation of individual TLC particle's 3D position, for the first time, using Astigmatism Particle Tracking Velocimetry (APTV).

Microfluidics has already revolutionized many aspects of science and technology but it will make an even bigger difference as the physics of fluids in small geometries are better understood. Experimental flow diagnostic methods have come a long way in the last decades but a reliable non-intrusive, 3D, temperature field measurement approach for micro flows remains an unsurpassed challenge. This is mainly due to the lack of availability of sensors that fit inside micro devices or droplets. Furthermore, existing non-intrusive optical measurement methods such as Laser Induced Fluorescence (LIF)[1,2] or TLC thermography[3,4] either use a light sheet (macroscopic setups) or illuminate the entire volume making it impossible to resolve 3D gradients in microscopic flows. However, estimating the 3D temperature field without bias errors due to spatial averaging is essential to better understand physical phenomena like Marangoni flows in droplets[5,6] or electrothermal micro vortices[7], as well as other multi physics phenomena.

A method is hereby proposed, to measure time-resolved temperature gradients in micro flows using TLC tracers whose position can be tracked in 3D. The first step in the process of accomplishing this task is the fabrication of an emulsion of TLC particles, with a narrow size distribution, which yields high quality color images that can be detected even when astigmatic abberations are introduced in the optical system. Micro encapsulated TLC particles have been the standard tool in the research community that has employed this measurement technique to measure flow temperatures. However, the size distribution of commercially available encapsulated TLCs is broad and the quality of individual particle images, at high magnifications, is far lower than that required for the tracking of their temperature, as can be seen in the top row of Figure 1[8]. Alternatively, an emulsion of non-encapsulated TLCs was produced at the Institute of Pharmaceutical Technology of the Braunschweig University of Technology using Shirasu Porous Glass Membrane emulsification (for further manufacturing information, see[8]) which produces a narrow size distribution of TLC micro spheres without polymer encapsulation. The absence of the polymer shell removes the bright reflected ring around the particles' cores, as observed in the second row of Figure 1, and yields particle intensity profiles that allow for the reliable detection of individual particles.

The images in rows 1 and 2 of Figure 1 were illuminated with a HXP 120 W flash lamp (other reports of TLC thermography experiments mention the use of Xenon, Halogen, and metal halide lamps, see Table 1 in[3]). Light bulbs in flash lamps, however, do not shine a homogeneous spectrum and exhibit pronounced intensity peaks in narrow wavelength bands, causing some colors to be scattered much more strongly than others, as is the case with the green band in rows 1 and 2 of Figure 1. This skews the temperature dependent color pattern and makes the temperature calibration a cumbersome task, not to mention the detection of differently colored particles in the same image.

† Electronic Supplementary Information (ESI) available: [details of any supplementary information available should be included here]. See DOI: 10.1039/b000000x/

Institut für Strömungsmechanik und Aerodynamik, Universität der Bundeswehr München, Werner-Heisenberg-Weg 39, 85577 Neubiberg, Germany. Fax: +49 (89) 6004 3896; Tel: +49 (89) 6004 2553; E-mail: rodrigo.segura@unibw.de

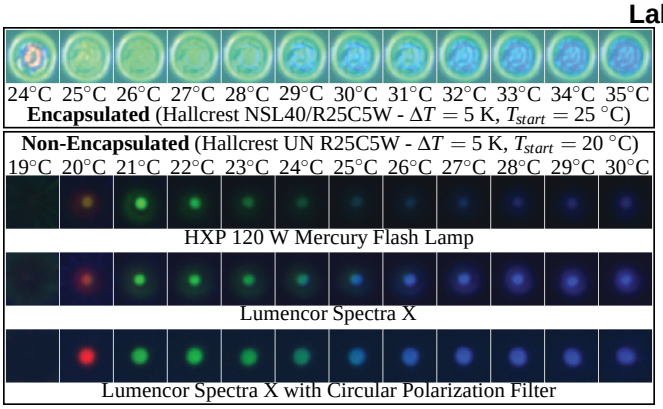

Fig. 1 Comparison of the particle images obtained with different illumination schemes for both encapsulated and non-encapsulated TLC particles with a temperature response range of 5 K.

Another leap forward in the technology of illumination sources was necessary to overcome this limitation. A so-called light engine was used instead of a high power flash lamp in order to illuminate the TLC particles with a more homogeneous spectrum. The Lumencor Spectra X light engine combines six solid-state light sources, filling the intensity deficiencies of flash lamps in specific color bands of the visible spectrum. Figure 1 shows the images of a non-encapsulated TLC particle illuminated with the the Spectra X. Despite the fact that the spectrum is not perfectly homogeneous, the improvement of the color signal speaks for itself, even when evaluated with the naked eye. Nevertheless, the intensity profiles of the particle change slightly with temperature, introducing a bias in the detection of their images' geometry, which is likely to increase for astigmatically defocused images. These halos that appear around bright green particles and, in a less pronounced fashion, around the blue shades of particles at higher temperatures, should be removed if the depth position is to be encoded in the elliptical geometry of defocused particles using Astigmatism Particle Tracking Velocimetry (APTV); in order for APTV to work, the intensity profiles of the particle images must not change as a function of temperature or color.

The solution to this issue involves the peculiar physics of the chiral nematic phase of liquid crystals, in which they manifest color scattering properties as a function of temperature. Molecules in chiral-nematic LCs, are arranged in layers with their long axes aligned parallel to each other. Moreover, the layers are parallel to the director (the average orientation of the molecules' long axes) which rotates from layer to layer causing a continuous rotation of the molecules along a helical path[9]. This meticulously ordered molecular structure grants chiral-nematic LCs unique optical properties, tabulated and thoroughly discussed in[4,10,11].

Among these properties, the following is of particular interest given that it allows for the design of a filter that transmits, almost exclusively, the temperature dependent wavelength bands scattered by the cores of the TLC particles. Chiral-nematic LCs are birefringent materials, meaning that their index of refraction changes as a function of polarization orientation and propagation direction. Furthermore, linearly polarized light that travels through them experiences an index of refraction, n, in the range between $n_{\min}$ and $n_{\max}$ which correspond to the cases when polarization orientation is perpendicular and parallel to the director, respectively. Furthermore, as explained by[12] (note that a stationary coordinate system was used when evaluating rotation chirality), type 'dextro' materials, as are TLCs, do not invert the chirality of circularly polarized light upon reflection from molecular layers. This is due to the fact that when polarized light travels from one layer to the next, the angle between its polarization plane and the director of the layer changes. This relative rotation causes one orthogonal component of the electric vector to experience a higher index of refraction while the other orthogonal component necessarily experiences a lower one. Consequently, only one of these components will experience a phase shift, thus inverting the reflected light's circular polarization chirality, which is normally opposite to that of the incident wave. In other words, light scattered by TLCs will always have a circular polarization chirality that matches the rotation of its molecular layers, regardless of the type of illumination that is shone upon them.

In order to take advantage of the optical properties of TLCs, a filter was designed, based on the method proposed by[13] to remove background noise, as well as unwanted reflections and halos that may surround the TLC particles' color-reflecting cores. The filter consists of a linear glass polarizer (Edmund Optics NT47-216), combined with an achromatic quarter wave plate (Melles Griot ACWP-400-700-06-4).

Figure 2 shows a schematic illustration of the circular polarization filter's operating principle. Assuming that the axis of the linear polarizer is aligned at 45° from the fast axis of the quarter wave plate, circularly polarized white light will be transmitted to the TLC particle seeded flow. Now, once the filter is aligned such that the circular polarization of transmitted light matches the rotation of the TLCs' molecular layers, the narrow wavelength bands reflected by the particle cores, will be transmitted back through the circular polarization filter, while all other light will be blocked by it. On the other hand, other reflections caused by index of refraction gradients or hard boundaries, such as those arising from the glass plate, the surface of the particles, walls or corners of microchip geometries, etc, will scatter light with an inverted circular polarization chirality. This light will be then transmitted by the quarter wave plate, but its transmitted polarization will cause the linear polarizer to block it from reaching the camera.

Unfortunately, achromatic quarter wave plates do not transmit perfectly circularly polarized light for all wavelengths, hence the background rejection is not perfect. Nevertheless,

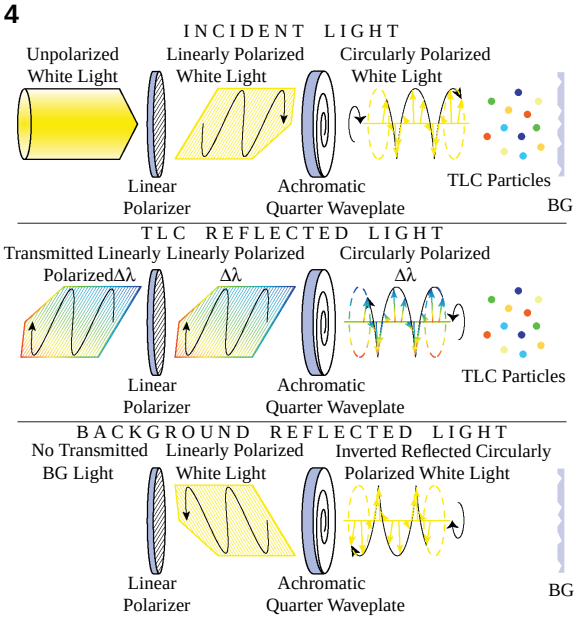

Fig. 2 Schematic of circular polarization filter.

though not optimal, the circular polarization principle improves the signal-to-noise ratio significantly, as illustrated in row 4 of Figure 1.

All in all, the final result of the combination of a balanced white light source with the circular polarization filter yields a substantial improvement in the acquisition of TLC color images, compared to the reports available in the literature so far. What is more, it allows for a more precise estimation of the particles' temperature as well as the use of defocusing methods, such as Astigmatism Particle Tracking Velocimetry (APTV), for the simultaneous time-resolved estimation of the particles' displacement and temperature in slow micro flows.

APTV is a recently developed defocusing method where the optical symmetry of the imaging system is broken by mounting a cylindrical lens between the imaging optics and the camera sensor[14–16]. The cylindrical lens focuses light in the y-axis, as does a conventional spherical lens, but acts as a flat window in the x-axis. The result are two different X-Z and Y-Z focal planes, F_{xz} and F_{yz}. What is more, spherical particles are projected as ellipses in an astigmatic imaging system, as opposed to the conventional circular images. The axes of the elliptical images, a_x and a_y can then be used to estimate and track the out-of-plane position of the particles in the measurement volume[7,15,17].

The depth position of the particles was calibrated by acquiring their defocused elliptical color images at different z positions. All experiments were performed at the microfluidics laboratory of the Bundeswehr University Munich (UniBw) with an Axio Observer Z.1 inverted microscope (Carl Zeiss AG) and a JAI AT-200 GE, 3CCD Progressive Scan RGB color camera. An LD Plan-NEOFLUAR, 20× objective lens was used along with a cylindrical lens with a focal length of $f_{cyl} = 500$ mm. Figure 3 shows a scatter plot of a_x vs a_y for all the particles detected during the calibration scan. Along with the plot of the data points, actual images of the particles at different z-positions are displayed in order to provide the reader a better understanding of the underlying pattern that allows for the estimation of the z-position from the geometry of the particle images. Now, as reported in[18], F_{xz} and F_{yz} are not actual flat planes in reality, nor are they perfectly parallel. For this reason, the elliptical image's geometry of a particle would vary for different (x,y) locations in the image, introducing a systematic error in the determination of the particle's z-position. To illustrate this effect, the smooth red and blue calibration curves were computed using the mean a_x and a_y of particle images (plotted as magenta and cyan colored circles, respectively) located in two different (x,y) regions of the image. Hence, it becomes clear why a single calibration curve for all detected particles introduces a substantial systematic error that can be corrected. In order to make this correction, two-dimensional square polynomial surface fits were calculated for both a_x and a_y distributions at each z-step of the calibration scan. This procedure provides a specific calibration curve for every (x,y) location in the image, thus compensating for the optical aberrations that cause the distortions in F_{xz} and F_{yz}. The z-position, z_i, of a particle image with elliptical axes, (a_{xi}, a_{yi}), was then determined by finding the point, $(a_x(z_i), a_y(z_i))$, along its respective calibration curve, that minimizes the Euclidean distance from (a_{xi}, a_{yi}).

A proof-of-concept experiment was performed in order to assess the viability of the method for real life applications.

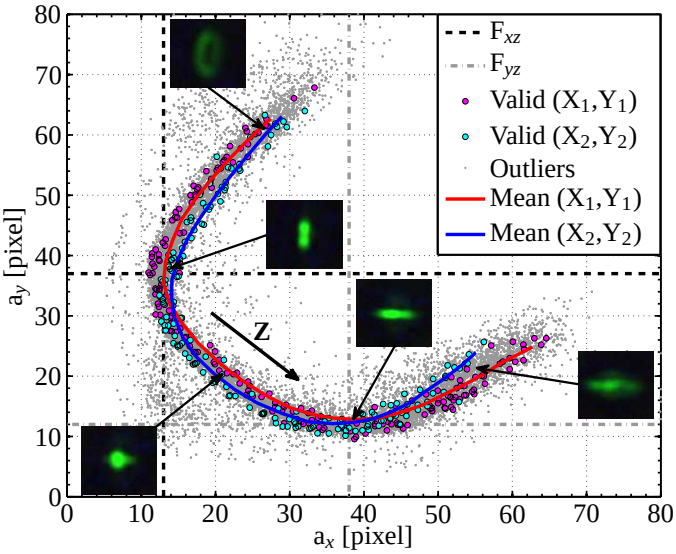

Fig. 3 Scatter plot of a_x vs a_y for valid particles detected during the calibration scan. Colored circles indicate valid particles in different (x,y) of the image and colored lines are smooth, interpolated mean (a_x, a_y) values at the temperatures covered in the calibration scan.

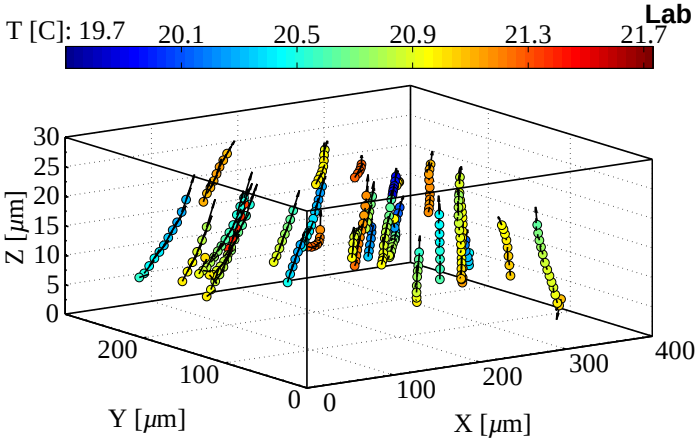

Fig. 4 TLC particle 3D motion inside a cooling droplet.

The rising flow in a small region of a warm water droplet was measured as it cooled down to room temperature. The temperature calibration was carried out by acquiring color images of the TLC particles at different temperatures and decorrelating the RGB data via proper orthogonal decomposition in order to perform a multi-variable calibration, using a system matrix, as outlined in[8]. Figure 4 shows the 3D particle tracks, along with their temperature, given by the colormap. A selection of trajectories detected during the cooling process are plotted to illustrate the capability of the method. Trajectories with different colors correspond to particles detected at different times during the measurement. The temperature calibration function is able to resolve the temperature decrease of individual particles as the droplet cools down, in this case allowing for a 3D Lagrangian analysis of the flow's temperature for the first time using individual tracer particles. Moreover, the particles clearly have a considerable velocity in the *z*-direction, as they migrate up and inwards. This depth component of displacement is not measured without astigmatism, which leaves a bias in the 2D tracking of the particles' motion.

The standard deviation from the true value, σ, of both the estimated 3D particle position and the particle temperature was calculated at each z and T steps of the respective calibration scans. For the temperature estimation, σ remained under 0.1 K throughout a temperature response range of 1.5 K (6.7%). It should be noted, however, that lower relative uncertainty values were observed for TLC materials with broader temperature response ranges (up to 20 K). Furthermore, the uncertainty of the temperature estimation was similar for measurements with and without astigmatism. This means that even though the particle images become dimmer when defocused, their SNR remained high enough to correctly interpret their color and estimate their temperature. On the other hand, the z-location estimation yielded σ values under 1.7 μm over a range of 20 μm (8.5%). The reason these uncertainty values are higher than those reported in the past for APTV measurements is that conventional APTV measurements use high-power lasers, as opposed to white light illumination, which yield much brighter particle images, whose geometry can be detected with better accuracy. Nevertheless, the proposed method allows for the quantitative evaluation of the 3D displacement and temperature gradient in the cooling droplet and opens the door to the possibility of evaluating 3D temperature and velocity fields in a myriad of microscopic setups.

The reader should note that even though the current state of technology did allow for the successful 3D temperature and displacement tracking of TLC particles in the droplet, limitations remain to be overcome in order to extend the applicability of the method to more complex microfluidics problems where higher velocities and weaker temperature gradients need to be resolved. Faster cameras with higher sensitivity, stronger light sources with a more homogeneous illumination spectrum, and TLC emulsions that yield better yet particle images are among the hardware improvements that are likely to happen in the near future and will substantially increase the impact of this measurement approach. That being said, the groundwork for a powerful method to simultaneously reconstruct 3D velocity and temperature fields in microscopic flows is laid out and proof of its functionality has been presented.

Acknowledgements

Financial support from the German Research Foundation (DFG) is acknowledged and appreciated, in the framework of the Research Unit FOR 856 and the Individual Grant KA 1808/8.

References

1 J. Coppeta and C. Rogers, *Experiments in Fluids*, 1998, **25**, 1–15.
2 J. Sakakibara and R. Adrian, *Experiments in Fluids*, 2004, **37**, 331–340.
3 D. Dabiri, *Experiments in Fluids*, 2009, **46**, 191–241.
4 I. Sage, *Liquid Crystals*, 2011, **38**, 1551–1561.
5 H. Hu and R. G. Larson, *Langmuir*, 2005, **21**, 3972–3980.
6 X. Xuefeng and J. Luo, *Applied Physics Letters*, 2007, **91**, 124102.
7 A. Kumar, C. Cierpka, S. J. Williams, C. J. Kähler and S. T. Wereley, *Microfluidics and Nanofluidics*, 2011, **10**, 355–365.
8 R. Segura, C. Cierpka, M. Rossi, S. Joseph, H. Bunjes and C. J. Kähler, *Microfluidics and Nanofluidics*, 2013, **14**, 445–456, open access.
9 J. L. Fergason, *Scientific American*, 1964, **211**, 77–85.
10 J. L. Fergason, *Molecular Crystals*, 1966, **1**, 293–307.
11 M. Parsley, *Handbook of thermochromic liquid crystal technology*, Hallcrest, Glenview, Il, 1991.
12 H. de Vries, *Acta Crystallographica*, 1951, **4**, 219–226.
13 M. Basson and T. S. Pottebaum, *Experiments in Fluids*, 2012, **53**, 803–814.
14 S. Chen, N. Angarita-Jaimes, D. Angarita-Jaimes, B. Pelc, A. H. Greenaway, C. E. Towers, D. Lin and D. P. Towers, *Experiments in Fluids*, 2009, **47**, 849–863.
15 C. Cierpka, R. Segura, R. Hain and C. J. Kähler, *Measurement, Science & Technology*, 2010, **21**, 045401.
16 M. Rossi and C. J. Kähler, *Experiments in Fluids*, 2014, **55**, 1–13.
17 P. B. Muller, M. Rossi, A. G. Marin, R. Barnkob, P. Augustsson, T. Laurell, C. J. Kähler and H. Bruus, *Physical Review E*, 2013, 023006.
18 C. Cierpka, M. Rossi, R. Segura and C. J. Kähler, *Measurement, Science & Technology*, 2011, **22**, 015401.